

Manjiroite or hydrous hollandite?

JEFFREY E. POST^{1,*}, PETER J. HEANEY², TIMOTHY B. FISCHER³, AND EUGENE S. ILTON⁴

¹Department of Mineral Sciences, Smithsonian Institution, P.O. Box 37012, Washington, D.C. 20013-7012, U.S.A.

²Department of Geosciences, Penn State University, University Park, Pennsylvania 16802, U.S.A.

³Chevron, 3901 Briarpark Drive, Houston, Texas 77042-5397, U.S.A.

⁴Pacific Northwest National Laboratory, 902 Battelle Boulevard, Richland, Washington 99352, U.S.A.

ABSTRACT

In this study, we investigated an unusual natural Mn oxide hollandite-group mineral from the Kohare Mine, Iwate Prefecture, Japan, that has predominantly water molecules in the tunnels, with K, Na, Ca, and Ba. The specimens are labeled as type manjiroite, but our analyses show that Na is not the dominant tunnel species, nor is it even the primary tunnel cation, suggesting either an error in the original analyses or significant compositional variation within samples from the type locality. Chemical analyses, X-ray photoelectron spectroscopy, and thermal gravimetric analysis measurements combined with Rietveld refinement results using synchrotron X-ray powder diffraction data suggest the chemical formula: $(K_{0.19}Na_{0.17}Ca_{0.03}Ba_{0.01}H_2O_{1.60})(Mn_{3.02}^{4+}Mn_{2.82}^{3+}Al_{0.14}Fe_{0.02})O_{13.47}(OH)_{2.53}$. Our analyses indicate that water is the primary tunnel species, and although water has been reported as a component in natural hollandites, this is the first detailed study of the crystal structure and dehydration behavior of a natural hydrous hollandite with water as the predominant tunnel species. This work underscores the rarity of natural Na-rich hollandite phases and focuses new attention on the role of hydrous components of hollandite-like phases in determining their capacities to exchange or accommodate various cations, such as Li^+ , Na^+ , Ba^{2+} , Pb^{2+} , and K^+ in natural systems.

Keywords: Hollandite, dehydration, Rietveld, manjiroite

INTRODUCTION

Manganese oxide minerals with hollandite-type structures and their synthetic analogs have long been studied for potential applications for storage of radioactive waste, ionic conductors, super capacitors, battery electrodes, and catalysts (Rossouw et al. 1992; Feng et al. 1995; Johnson et al. 1997; Kijima et al. 2005; Sauvage et al. 2007; Bruce et al. 2012; Zhang et al. 2012; Tompsett and Islam 2013; Yang et al. 2015, 2017). The Mn hollandite-group minerals occur in oxidized zones of Mn-rich deposits, in low-temperature hydrothermal veins, and as sedimentary cements and coatings, including dendrites and nodules. Some studies suggest they might also form as alteration products from biogenic Mn oxides (Grangeon 2015; Carmichael et al. 2017).

Hollandite-group Mn oxide structures consist of double chains of edge-sharing Mn^{4+} -O octahedra that corner-share with other double chains to form a framework containing large tunnels (Fig. 1). The tunnels are partially filled with large univalent or divalent cations and sometimes water molecules, and the dominant cation determines the particular mineral phase, e.g., K^+ (cryptomelane), Na^+ (manjiroite), Ba^{2+} (hollandite), Pb^{2+} (coronadite), and Sr^{2+} (strontiomelane). Lower-valence cations (e.g., Mn^{3+} , Al^{3+} , Fe^{3+} , etc.) substitute for some of the Mn^{4+} to offset the positive charge of the tunnel cations. Mn hollandite minerals typically contain a variety of tunnel cations. The

framework dimensions and consequent tunnel cation coordination environment apparently favor K, Ba, and Pb; smaller divalent cations such as Mg and Ca are rare in Mn hollandite-group minerals (Feng et al. 1995). Na is a common minor constituent in cryptomelane, but manjiroite is apparently rare. Hollandite phases with only divalent tunnel cations typically have half-filled tunnel sites, with cations ordered every other unit cell along the tunnels, and in those with predominantly K and Na, the tunnel sites can be as much as two-thirds to three-quarters filled. Detailed structure refinements have been reported for hollandite and cryptomelane (Post et al. 1982), coronadite (Post and Bish 1989), and strontiomelane (Meisser et al. 1999). Analogous minerals are known with Fe^{3+} , e.g., akageneite (Post and Buchwald 1991; Post et al. 2003), and Ti^{4+} (Post et al. 1982; Szymański 1986) as the primary octahedral cations.

In this study, we investigated an unusual natural Mn oxide hollandite phase from the oxidized zone of a rhodochrosite-tephroite-rhodonite bedded deposit at the Kohare Mine, Iwate Prefecture, Japan that has predominantly water molecules in the tunnels, with K, Na, Ca, and Ba. Chemical analyses, X-ray photoelectron spectroscopy (XPS), and thermal gravimetric analysis (TGA) measurements combined with Rietveld refinement results using synchrotron X-ray powder diffraction data suggest the approximate chemical formula: $(K_{0.19}Na_{0.17}Ca_{0.03}Ba_{0.01})(Mn_{3.02}^{4+}Mn_{2.82}^{3+}Al_{0.14}Fe_{0.02})(O,OH)_{16} \cdot nH_2O$. Interestingly, the specimens studied here are labeled as type manjiroite used by Nambu and Tanida (1967) for their original mineral description, but our analyses show that Na is not the dominant

* E-mail: postj@si.edu

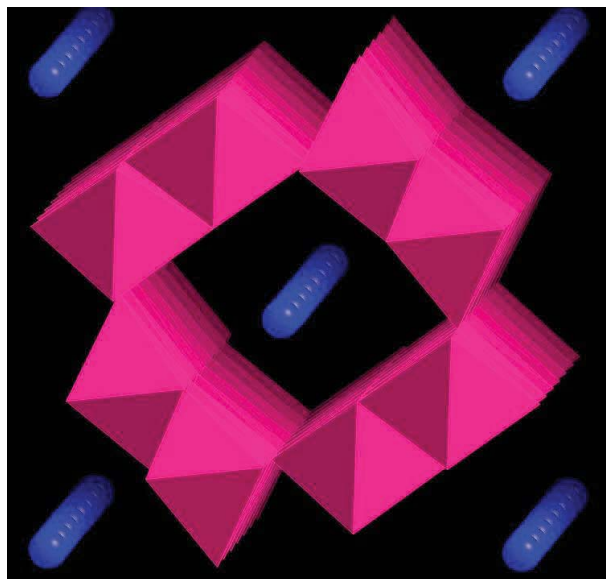


FIGURE 1. Polyhedral representation of the hollandite structure, consisting of double chains of $(\text{Mn}^{2+}, \text{Mn}^{3+})\text{O}_6$ octahedra; the spheres represent the tunnel cations. (Color online.)

tunnel species, nor is it even the primary tunnel cation. It is, of course, possible that the samples studied here, despite the type designation, are different from the sample analyzed by Nambu and Tanida (1967), but the discrepancies motivate a more thorough characterization of the samples. Moreover, our analyses indicate that water is the primary tunnel species, and although water has been reported as a component in natural hollandites, this is the first detailed study of the crystal structure and dehydration behavior of a natural hydrous hollandite with water as the predominant tunnel species.

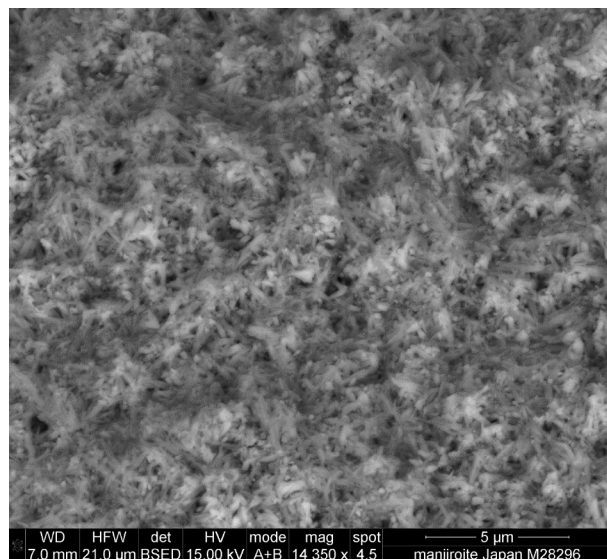


FIGURE 2. Backscattered electron microscope image of the type manjiroite specimen. Individual crystals are approximately $0.5 \times 4 \mu\text{m}$.

EXPERIMENTAL METHODS

Sample and chemical analyses

The primary sample used for this study, M28296 (National Museum of Nature and Science -Japan) from the Kohare Mine, Iwate Prefecture, Japan, is labeled as a portion of the type manjiroite used by Nambu and Tanida (1967). Scanning electron microscope (FEI Nova NanoSEM 600; Department of Mineral Sciences, Smithsonian Institution) images revealed the sample to be polycrystalline consisting of a fine mesh of $\sim 0.5 \times 4 \mu\text{m}$ fiber-like crystals (Fig. 2), consistent with the description of the sample studied by Nambu and Tanida (1967)—as dense compact masses showing a conchoidal fracture. Electron microprobe analyses (JEOL JXA8900R, operated at 15 keV) were performed using samples embedded in epoxy, polished and carbon-coated. A defocused electron beam was used to minimize any Na loss during analyses.

A portion of the sample was submitted for instrumental neutron activation analysis (INAA) at the University of Missouri-Columbia Research Reactor Center. Two ~ 40 mg samples were analyzed for Na and K using NIST standard reference materials SRM 688 (basalt rock) for calculating Na concentrations and SRM 1633b (coal fly ash) for K. Samples were irradiated for 60 s and allowed to decay for ~ 48 h, and live-time counted for 1 h. The Na concentrations were quantified using the net peak area of the 1368 keV γ -ray from the decay of ^{24}Na ($t_{1/2} = 14.96$ h), which was produced via the neutron capture by ^{23}Na , and the K concentrations were quantified using the net peak area of the 1524 keV γ -ray from the decay of ^{42}K ($t_{1/2} = 12.36$ h), which was produced via the neutron capture by ^{41}K .

We also analyzed a small portion of a second sample from the private collection of Kinichi Sakurai that was labeled as “type manjiroite from Dr. Nambu.” The physical appearance was the same as the original sample, and it was mounted, polished, and carbon-coated for electron microprobe analysis.

X-ray diffraction

The sample used for X-ray diffraction was hand-ground under acetone in an agate mortar and passed through a 325-mesh sieve and loaded into 0.7 mm quartz-glass (NSLS) or 1 mm (ID) polyimide (APS) capillaries. XRD data were collected: (1) at beamline X7B of the National Synchrotron Light Source (NSLS), Brookhaven National Laboratory (BNL), using a wavelength of 0.3184 Å and a MAR345 full imaging plate detector, and (2) at beamline 11BM at the Advanced Photon Source, using a wavelength of 0.414211 Å.

The synchrotron heating experiment was performed at NSLS in air using a Blake Instruments furnace with a Pt-13%Rh coiled wire yoke encased in ZrO_2 cement (Brown et al. 1973). The temperature was varied with an Omega controller and monitored with a Chromel-Alumel thermocouple located ~ 2 mm from the specimen. The actual sample temperature was calibrated for the range 25 to 1000 °C by a variety of phase and melting transitions and by the placement of an additional thermocouple in the sample position. The highly linear relationship between the observed and actual temperatures ($R^2 = 0.983$) allowed us to calculate a calibration curve with an estimated error of ± 5 °C for a given temperature. Temperature-resolved data from 27 to 800 °C were collected as a series of 120 s exposures. The temperature was increased continuously at 6.4 °C/min, and measurements were obtained every ~ 25 °C, because of down time for repositioning of the sample and reading the imaging plate; thus, each exposure encompassed a temperature range of ~ 13 °C. During each exposure, the sample was rotated through a 120° angle. Preferred orientation of the powder was eliminated through a combination of the specimen rotation, use of a capillary sample holder, and full intensity integration of the diffraction rings, as obtained using the program Fit2D (Hammersley et al. 1996) with a polarization factor of 0.93.

Rietveld refinements (Rietveld 1969) were performed for selected diffraction patterns using the General Structure Analysis System-II (GSAS-II) software (Toby and Von Dreele 2013). Diffraction data generated by a LaB_6 standard (NIST SRM 660a) were used to calibrate peak profile parameters that described instrumental broadening. For all samples, diffraction peak profiles were fit with a pseudo-Voigt function as parameterized by Thompson, et al. (1987) and microstrain anisotropic broadening terms by Stephens (1999).

The initial atom positions for the refinements were those for cryptomelane (space group: $I2/m$) reported by Post et al. (1982). Only background parameters, scale factor, unit-cell parameters, and peak profile coefficients were varied in the initial refinement cycles; background intensities were fitted with a Chebyshev function using 5–7 terms. After convergence, atom positions and occupancy factor of the tunnel water O atom were refined. Atomic displacement factors, other than for the water O, were fixed to typical values for hollandite-like structures, e.g., Post et al. (1982). The final refinement parameters for RT hydrous hollandite, using the APS 11BM data and selected bond distances, are reported in the Online Materials¹ CIF. The final observed, calculated, and difference patterns are plotted in Figure 3.

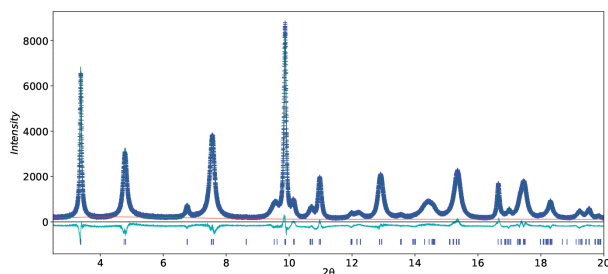


FIGURE 3. Final observed (crosses), calculated (solid line), and difference (below) powder X-ray diffraction patterns from the Rietveld refinement for “hydrous hollandite.” The Bragg reflections are marked by the set of small vertical lines. (Color online.)

Fourier transform infrared spectroscopy (FTIR)

Samples were disaggregated under acetone in a mortar and pestle and sieved through a 325-mesh sieve; 0.5 to 1 mg manjiroite samples were milled with ~250 mg KBr using a SPECAC ball mixing mill for 1–2 min and pressed into pellets. Transmission vibrational spectra were collected for a range of 400 to 4000 cm^{-1} on a Nicolet 6700 analytical FTIR spectrometer. The resolution was set at 3.86 cm^{-1} , and 64 scans were co-added for each spectrum. The Omnic 8 software (Nicolet) was used to view data during data collection.

X-ray photoelectron spectroscopy (XPS)

For XPS analysis, data collection and fitting procedures were followed as reported by Ilton et al. (2016). Powder samples were mounted on strips of conductive copper tape affixed to copper stubs and then pressed with clean borosilicate glass blocks onto copper stubs. Measurements were conducted with a Kratos Axis Ultra DLD spectrometer with an AlK α X-ray source (1486.7 eV) operating at 10 mA and 15 kV. Magnetic immersion lenses were used to improve collection efficiency. The instrument work function was calibrated to give a binding energy (BE) of 83.96 ± 0.05 eV for the $4f_{7/2}$ line of metallic gold. The spectrometer dispersion was adjusted to yield a BE of 932.62 eV for the $\text{Cu}2p_{3/2}$ line of metallic copper. Measurements of the Mn2p, Mn3s, Mn3p, O1s, C1s, and various alkali and alkaline earth lines were conducted with a step size of 0.1 eV, an analysis area of $300 \times 700 \mu\text{m}$, and pass energies (PE) of 20 or 40 eV. The resultant full-width-at-half-maximums (FWHM) for the $\text{Ag}3d_{5/2}$ line were 0.54 and 0.77 eV, respectively. The low sensitivity of the Mn3s line resulted in measurements only with PE = 40 eV. Survey scans were conducted at PE = 160 eV and step size = 0.5 eV. XPS spectra were fit by non-linear least squares after Shirley background subtractions with the CasaXPS curve resolution software package. Gaussian/Lorentzian contributions to line shapes were numerically convoluted with a Voigt function.

Thermogravimetric analyses

The dehydration behavior was investigated by measuring H_2O and O_2 loss using combined thermal-gravimetric analysis and mass spectroscopy (TGA-MS). Samples were analyzed on a TA Instruments Discovery TGA 55 connected to a mass spectrometer. Calcium oxalate monohydrate ($\text{CaC}_2\text{O}_4 \cdot \text{H}_2\text{O}$) was used as a standard for calibration of the TGA and MS. Two types of analysis runs were performed, both using about 9 mg of sample. In the first, the sample was heated at 10 $^\circ\text{C}/\text{min}$ to a temperature of 250 $^\circ\text{C}$, then held for 1 h before continued heating to 950 $^\circ\text{C}$ at the same rate. In the second experiment the sample was heated continuously to 950 $^\circ\text{C}$. Mass spectra at 18 (H_2O) and 32 (O_2) were collected continuously during each experimental run and then integrated over 100 points to determine the differential thermal gravimetric (DTG) curves.

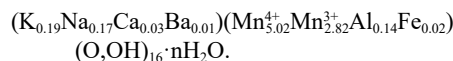
RESULTS AND DISCUSSION

Characterization of type “manjiroite” samples

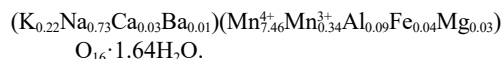
The XPS results for Mn showed 64.3 mol% Mn^{4+} , 35.7 mol% Mn^{3+} , and no Mn^{2+} , indicating an average Mn oxidation state of +3.66. Similar values, 62 mol% Mn^{4+} and 38 mol% Mn^{3+} , were derived using the Rietveld refinement mean Mn-O octahedral bond distance of 1.934 Å, assuming Shannon (1976) ideal bond

lengths: $\text{Mn}^{4+}\text{-O} = 1.89 \text{ Å}$ and $\text{Mn}^{3+}\text{-O} = 2.005 \text{ Å}$. Additionally, linear combination fitting to the X-ray absorption spectroscopy Mn absorption edge yielded 64 mol% Mn^{4+} and 36 mol% Mn^{3+} (unpublished results).

Electron microprobe analyses were generally consistent with the chemical formula reported by Nambu and Tanida (1967), except that we detected significantly less Na. Utilizing Mn oxidation states determined by XPS, we derived the following formula:



For comparison, Nambu and Tanida (1967) report:



The Na and K concentrations that we measured by neutron activation (0.23 K and 0.15 Na per 16 O atoms) were within the range of our electron microprobe measurements.

It is possible that material labeled as “type” is not homogeneous, and the sample used here has less Na than the specimen used in the 1967 study, but it seems curiously coincidental that the concentrations of the other elements match so well. Alternatively, the high-Na value in the earlier analysis was in error. This possibility is supported by the fact that the short 2.85 Å spacing between adjacent sites along the tunnels in hollandite phases generally limits the total number of tunnel species (cations plus water molecules) to fewer than two per unit cell and the total from the Nambu and Tanida (1967) formula is an unlikely high value of 2.63.

The electron microprobe analysis of the “type manjiroite” from the Sakurai collection yielded the formula:



similar to that determined for our original sample, with the exception of a higher concentration of K. The low concentration of Na in this sample also is inconsistent with the definition of manjiroite, but the analyses support some chemical variation among samples labeled as “type manjiroite.” We did not have sufficient sample to determine either the water concentration or the $\text{Mn}^{3+}/\text{Mn}^{4+}$ ratio.

Our XPS results for the sample from the Kohare Mine (36% Mn^{3+}) indicated that there are 2.82 Mn^{3+} (out of 7.84 Mn) per unit cell (16 O atoms), which together with the 0.14 Al^{3+} and 0.02 Fe^{3+} yields a net 2.98 negative charge on the Mn-O octahedral framework. By comparison, the total tunnel cation charge from the chemical formula is +0.44, resulting in an overall charge deficit of −2.54. The absence of any other cations in the chemical analyses suggests that charge balance likely is achieved by replacing 2.54 of the 16 framework O per unit cell by OH^- (15.9%). This assumption is supported by the fitting results of the XPS O spectra that indicated predominantly atomic O with significant amounts of OH and H_2O . Alternatively, some studies of synthetic hydrous hollandite-like phases speculated that hydronium cations might be important tunnel species (Bruce et al. 2012; Yang et al.

2017), instead of or in addition to molecular water, but our XPS spectra did not show evidence of significant H_3O^+ .

The FTIR spectrum collected for manjiroite at 25 °C is plotted in Figure 4 and shows a moderately intense broad peak between ~ 3000 and 3600 cm^{-1} and one near 1600 cm^{-1} . Potter and Rossman (1979) observed that many hollandite-group mineral samples exhibited similarly, but typically low-intensity, broad FTIR absorption features and assigned them to OH stretch and water bending modes, respectively. They also concluded that the broadness of the bands is characteristic of O-H stretch vibrations associated with disordered molecular water and OH $^-$.

Although the samples studied here, and possibly that analyzed by Nambu and Tanida (1967), may not properly be classified as the Na-dominant variety of hollandite defined as manjiroite, the new analyses nonetheless confirm that this material is novel. Typical analyses of Ba- or Pb-rich hollandite-type minerals show about one tunnel cation per unit cell, and for cryptomelane, the number of K can be as high as 1.5 cations per unit cell. The total number of tunnel cations per unit cell determined in the present study is an anomalously low 0.44–0.46 for the first and 0.60 for the second sample. The water analyses reported by Nambu and Tanida (1967), and those from the current TGA study discussed below, suggest that H_2O molecules are the predominant tunnel species, making this mineral not manjiroite but a “hydrous hollandite” (or perhaps, considering that K is the primary tunnel cation, a “hydrous cryptomelane”).

X-ray diffraction and Rietveld refinement

The Rietveld refinements showed that the Mn and O positions in the octahedral framework are similar to those reported for cryptomelane by Post et al. (1982). The atom positions and other Rietveld refinement results are summarized in the CIF¹. A Fourier difference map calculated using a structure model with only framework Mn and O atoms showed a diffuse area of electron density centered at the special position at (0,0,0) in the centers of the tunnels and extending along the length of the tunnel, consistent with the water molecules and tunnel cations positionally disordered about (0,0,0). A single-crystal X-ray diffraction study of cryptomelane by Post et al. (1982) concluded that large cations such as K (and Ba^{2+}) occupy positions at or near the special position where they are close to the preferred K-O bond distance of $\sim 2.90\text{ Å}$ from eight O atoms. They also suggested that smaller cations (e.g., Na^+) are displaced off the special position along the tunnel, where they form shorter and more favorable bonds with the nearest framework O atoms.

During the refinement in the present study, the K was placed at (0,0,0) and the occupancy fixed to the analytical value, and an O atom (representing water and Na) was placed at (0,y,0), and its position and occupancy refined. As the difference map indicated that the electron density extended in the tunnel direction, the water O was modeled using an anisotropic temperature factor with only the U_{22} (tunnel direction) component refined, yielding values in the range 0.02 to 0.04, and fixed to 0.025 for the final refinement cycles. The refined occupancy factor for the O site, after accounting for the Na (and Ba and Ca), indicated ~ 1.7 water molecules per unit cell, close to the value of 1.64 reported by Nambu and Tanida (1967). An accurate determination of the tunnel site occupancy factor was complicated by the positional disorder, and correlations

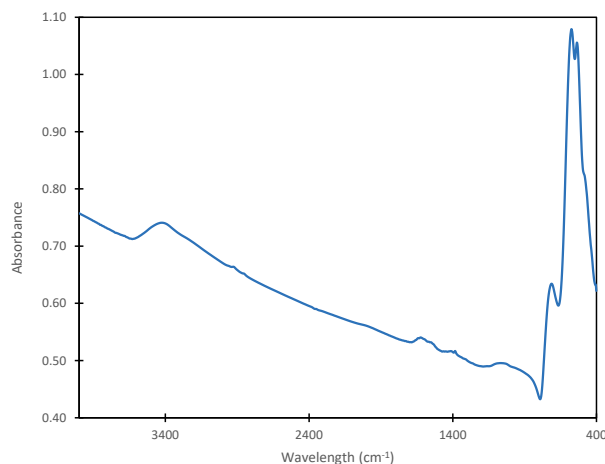


FIGURE 4. FTIR spectrum for “hydrous hollandite.” (Color online.)

with background coefficients and thermal displacement factors. The analysis total of ~ 0.40 tunnel cations plus 1.60 water molecules would fill the two tunnel sites per unit cell.

The K^+ at the special position at (0,0,0) is 2.91 Å from four O3 atoms and 2.86 Å from four O1 atoms, and these distances compare well with the 2.90 Å K-O bond length predicted by Shannon (1976). It is, therefore, likely that the refined satellite tunnel position, which is $\sim 0.45\text{ Å}$ from the special position, is primarily occupied by water O and Na. By displacing along the tunnel, they form shorter and more favorable distances of 2.66 Å from two O1 atoms and 2.71 Å from two O3 atoms; typical Na-O bonds are 2.6 Å (Shannon 1976), and water H-bonds are $\sim 2.7\text{ Å}$ (Baur 1972).

Although the Rietveld refinement results suggest that our model reasonably describes the electron density in the tunnels, the actual situation is certainly more complex, and in fact, significant positional disorder is indicated by the large and diffuse area of electron density on the difference Fourier map. The chemical analyses show that K^+ occupies only one out of every four or five sites along a given tunnel, and likely the position of water molecules or Na^+ will be different depending upon whether the adjacent special position is filled or empty. Additionally, water molecules will adjust as they form H-bonds with each other and perhaps with framework OH $^-$. DFT modeling by Bruce et al. (2012) for a synthetic hydrous hollandite-like ($\alpha\text{-MnO}_2$) phase [$(\text{H}_2\text{O}, \text{H}_3\text{O}^+)_{0.17}\text{MnO}_2$] showed that numerous different water molecule orientations and positions yielded similar energies, suggesting that the water species are disordered in the tunnels. Finally, structure energy calculations for hollandite-like phases by Post and Burnham (1986) noted that the particular local arrangements of Mn^{4+} and Mn^{3+} in the octahedral sites also affect tunnel cation positions. All of this suggests that the tunnel sites used for the refinement are at best an average of what are likely numerous local tunnel species configurations.

The time-resolved synchrotron X-ray diffraction patterns collected while heating the “manjiroite” sample from 24 to 900 °C are plotted in Figure 5, and unit-cell parameters determined for selected temperatures by Rietveld refinements are plotted in Figure 6. These results indicate a structural adjustment between 200 and 300 °C , associated with decreases in a and c , and unit-cell volume and a slight increase in β , which coincides with the

loss of tunnel water observed in the dehydration experiments discussed below. A steady increase in a , c , β , and unit-cell volume above $\sim 400^\circ\text{C}$, is associated with the breakdown of the hollandite structure and release of O and OH, as discussed below. The diffraction data show that bixbyite (Mn_2O_3) forms above $\sim 600^\circ\text{C}$. Previous heating experiments on hollandite-like phases suggested that the types and numbers of tunnel species affect the temperatures for the initial formation of bixbyite. Akkopru-Akgun et al. (2015), for example, reported that the transition temperature varied from 600 to 675°C as the Ba:Mn increased from 0.04 to 0.1, which is consistent with our observed 600°C transition temperature and total tunnel cation to Mn ratio of 0.05.

Thermogravimetric analyses

The TGA/DTG-MS data (Fig. 7) revealed that the total weight loss of water and O_2 from RT to 950°C for the Kohare Mine manjiroite was $\sim 14\text{ wt}\%$. This value compares well with the total anticipated weight loss of $13.3\text{ wt}\%$ based on the chemical formula that we derived using EPMA, Rietveld refinements, and XPS data from this study. During the TGA heating trials, three significant weight loss events were apparent at ~ 250 , 475 , and 650°C . The O_2 loss above $\sim 450^\circ\text{C}$ coincides with the breakdown of the hollandite structure and subsequent transformation to bixbyite (Mn_2O_3). A relatively sharp $\sim 3\text{ wt}\%$ water loss peak was evident at $\sim 250^\circ\text{C}$, and a second more gradual water loss occurred at $\sim 425^\circ\text{C}$, coincident with the initial O_2 emission. The loss of $\sim 0.5\text{ wt}\%$ H_2O below $\sim 200^\circ\text{C}$ is assumed to be surface adsorbed water.

The mass spectrometer curves in Figures 7b indicate that the weight loss event at $\sim 250^\circ\text{C}$ derived primarily from water,

likely corresponding to the evolution of tunnel molecular water. If we assume there are $1.56\text{ H}_2\text{O}$ per unit cell, the theoretical weight loss for Kohare Mine manjiroite is $3.7\text{ wt}\%$, close to our observed value of $\sim 3.5\text{ wt}\%$, ($3\text{ wt}\%$ at $\sim 250^\circ\text{C}$ plus $0.5\text{ wt}\%$ below 200°C) and that of $3.9\text{ wt}\%$ $\text{H}_2\text{O}(+)$ reported by Nambu and Tanida (1967). Our conclusion is consistent with the observation by Feng et al. (1995) that structural water was released below 350°C from a synthetic hollandite-like phase, $(\text{H}_2\text{O})_{0.21}\text{MnO}_2$. Also, Bruce et al. (2012) reported tunnel water loss between ~ 260 and 380°C for synthetic $(\text{H}_2\text{O}, \text{H}_3\text{O}^+)_{0.17}\text{MnO}_2$, and Yang et al. (2017) noted that tunnel water was removed from a similar phase by 400°C .

The plots in Figure 7 reveal that the second weight-loss event between 300 and 575°C is caused by overlapping H_2O and O_2 emissions. The water loss occurs from 300 to 475°C , with the DTGA peak at about 425°C . The gradual loss, as indicated by the greater breadth of this mass spectrometer peak relative to that at 250°C , and the overlapping O_2 emission ranging from ~ 375 to 600°C (centered at 490°C) suggest that this event resulted from the release of framework OH. This interpretation is consistent with the XRD data that show a breakdown of the hollandite structure above $\sim 400^\circ\text{C}$, and with dehydration experiments by Feng et al. (1995) that showed a similar release of O_2 and H_2O from $(\text{H}_2\text{O})_{0.21}\text{MnO}_2$ at $\sim 480^\circ\text{C}$.

As indicated above, comparison of the total tunnel cation charge of $+0.44$ with the deficit on the Mn-O framework, assuming $34\%\text{ Mn}^{3+}$ as measured by XPS, indicates that 2.53 OH^- are required for overall charge balance. The expected $3.1\text{ wt}\%$ water loss corresponding to this number of hydroxyl anions is in the range of the observed ~ 3 to $4\text{ wt}\%$. The overlap of the H_2O and

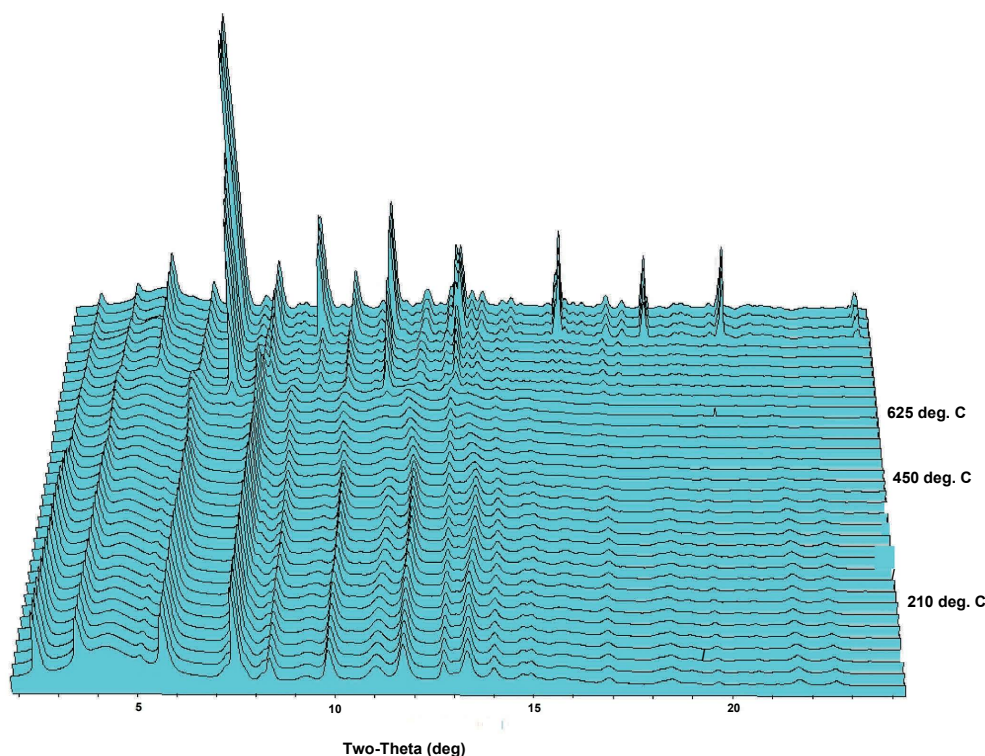


FIGURE 5. Synchrotron powder X-ray diffraction patterns vs. temperature from RT (front) to 800°C . (Color online.)

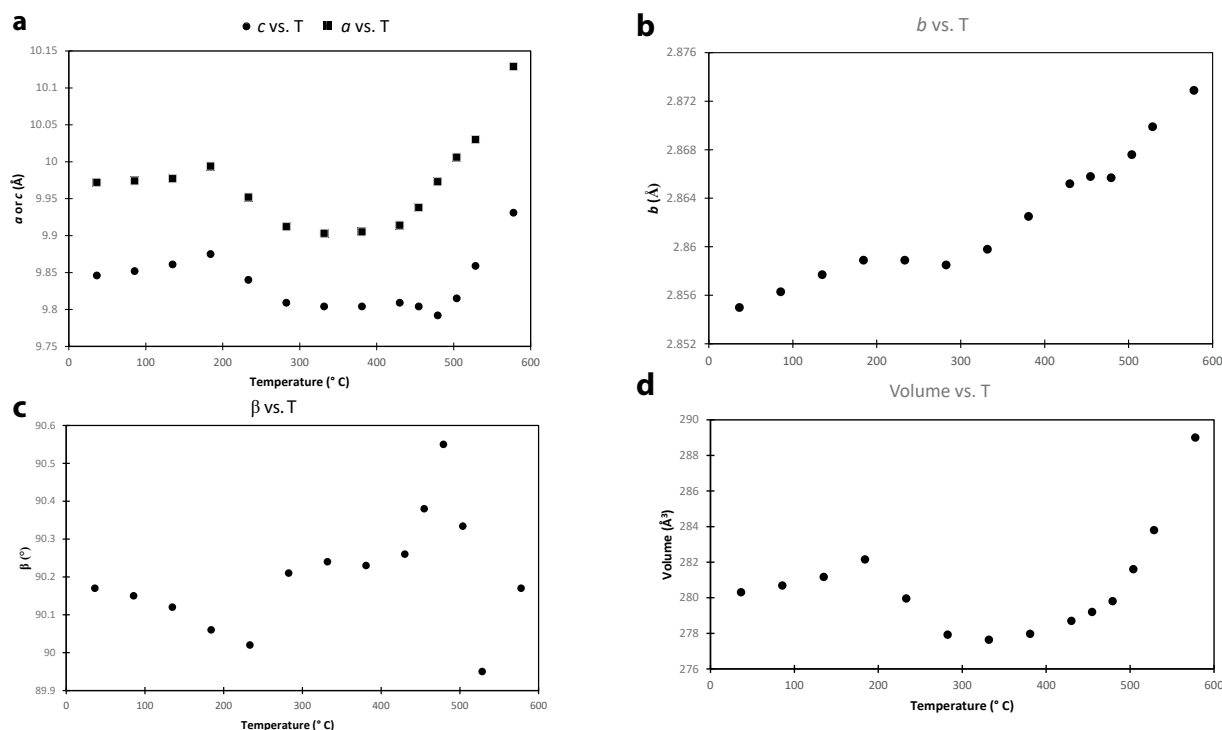


FIGURE 6. Plot of (a) a and c , (b) b , (c) β , and (d) unit-cell volume for "hydrous hollandite" for the temperature range 27 to 800 °C. Calculated e.s.d. values fall within the areas of the plotting symbols.

O₂ emissions prevents a more precise determination of actual water loss in this event.

The O₂ emission peak at 650 °C coincides with the transformation to bixbyite, with the concomitant reduction of Mn⁴⁺ to Mn³⁺. In our X-ray diffraction heating experiments, the first bixbyite peaks appeared at 601 °C. The origin of the second

O₂ emission at ~750 °C is not clear. It might be related to the breakdown of a remnant oxide phase formed by the tunnel cations (K⁺ and Na⁺) and the octahedral Al and Fe with Mn as the hollandite structure transformed to bixbyite. Previous studies have suggested that a Na or K spinel-type Mn oxide might form as intermediate phases before eventual transformation to bixbyite

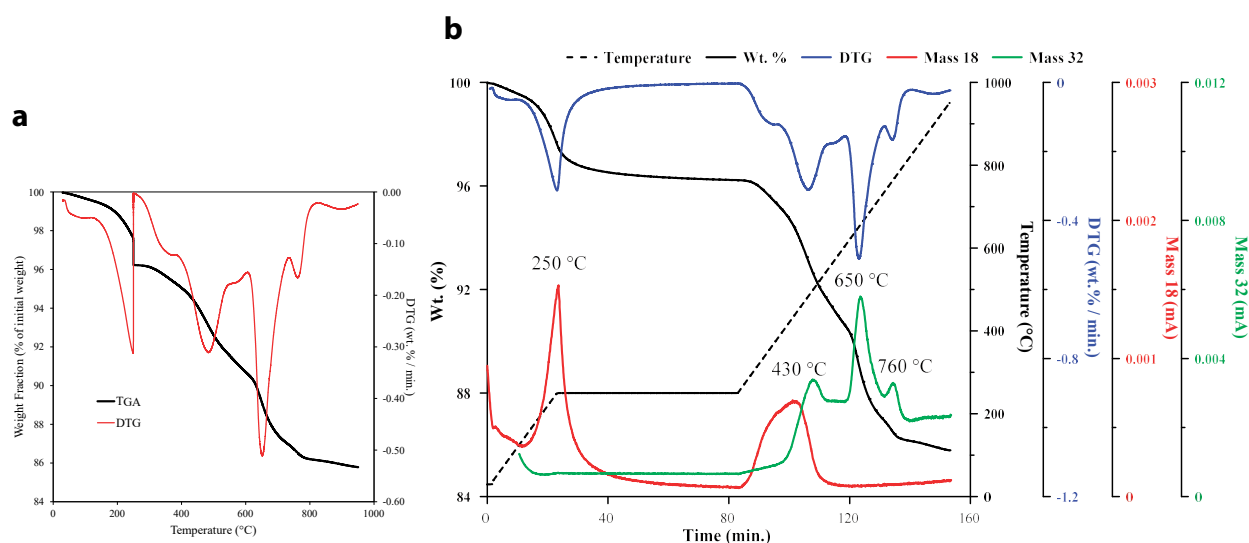


FIGURE 7. Results of heating/dehydration experiments for "hydrous hollandite": (a) mass loss (TGA) and differential mass loss (DTG) vs. temperature, and (b) mass loss of sample and mass spectrometer H₂O (18) and O₂ (32) loss vs. temperature of experiment with one-hour hold at 250 °C. (Color online.)

(Feng et al. 1995), although a spinel-like phase was not apparent from our XRD analyses.

Manjiroite or “hydrous hollandite”?

The “type manjiroite” samples analyzed for this study did not conform to the chemical composition ascribed to manjiroite by Nambu and Tanida (1967) in their new mineral description. Although some chemical variation was apparent for the two “type” samples interrogated here, the Na concentrations were similar. Since both exhibited K as the primary tunnel cation, they should not be classified as manjiroite. We are not able to explain the discrepancy between our results and those of the original study. The analyses by Nambu and Tanida (1967) were performed using wet chemical methods, but details sufficient to evaluate the results were not provided. This work does, however, underscore the relative scarcity of manjiroite. Other than the original report by Nambu and Tanida (1967), the only confirmed manjiroite occurrence of which we are aware is that reported by Gutzmer and Beukes (2000) from the South African Kalahari manganese field. Our own analyses of samples from that locality confirm that Na is the primary tunnel species (unpublished results). Another purported locality for supposed “manjiroite” specimens in many museums and private collections is Tombstone, Arizona. We have analyzed dozens of such samples from a variety of sources over the past several years, and none are manjiroite; most are cryptomelane, sometimes with coronadite (unpublished results).

The naming convention for hollandite-group minerals dictates that the Kohare Mine samples analyzed in this study would be called cryptomelane since K is the primary tunnel cation. On the other hand, this material is unusual because molecular water rather than cations are the predominant tunnel species. Hollandite species nomenclature does not consider the role of tunnel water, even though it is a common constituent in many natural hollandite-group phases. Gruner (1943) attempted to clarify the confusion related to the hollandite-group classification by proposing a general formula that includes molecular water, but the International Mineralogical Association has not adopted his nomenclature. Other studies (Nambu and Tanida 1980) noted that hollandite minerals that experienced low to moderate metamorphism generally have low-water contents (<1 wt%), whereas those that form hydrothermally or in sediments can have significant structural water. Because of uncertainties associated with analyzing hollandite-group minerals, such as unknown Mn oxidation states, fine-grained textures, and sample inhomogeneities, low-electron microprobe analysis totals are routine. Therefore, estimates of water by difference commonly are problematic. Unless TGA, FTIR or other water measurements are made, the presence of water might be overlooked or ignored.

Materials scientists have long been interested in α -MnO₂ (hollandite structure) with predominantly, or all, H₂O in the tunnels—so-called “hydrous hollandite” (Rossouw et al. 1992; Feng et al. 1995; Johnson et al. 1997; Yang et al. 2015, 2017). Because hydrous hollandites readily exchange H⁺ and H₂O (or H₃O⁺) for Li and certain other cations, it is being investigated as an effective precursor for ion insertion reactions to create hollandite-structure battery electrodes (Kijima et al. 2005; Sauvage et al. 2007; Yang et al. 2017).

This study confirms that analogs to synthetic hydrous hollandites occur naturally. Chemical analyses, Rietveld structure re-

finement, and heating experiments all indicate that for the samples studied here the tunnels were approximately three-quarters filled with water molecules, with only minor quantities of K, Na, Ca, and Ba. Additionally, ~15 mol% of the octahedral O atoms was OH⁻, making this a truly soggy hollandite-like phase.

IMPLICATIONS

Our study raises questions about the material originally described as manjiroite by Nambu and Tanida (1967), suggesting that either there is considerable variation of the Na concentration in the type locality samples or an error in the original analyses. Although the low-Na concentrations in the samples studied here ruled out a classification as manjiroite *sensu stricto*, they nevertheless represented a novel hydrous hollandite-like mineral. As such, they provided the opportunity for the first detailed characterization of the structure and dehydration behavior of a natural hollandite-like mineral with molecular water as the predominant tunnel species—filling approximately three-quarters of the tunnel sites. This work focuses new attention on the role of molecular water in hollandite minerals, especially those formed from, or associated with, low-temperature aqueous systems. Studies of synthetic hydrous hollandites suggest that structural water affects their cation-exchange properties. In particular, higher amounts of water promote the insertion of Li and other smaller cations into the tunnels (Yang et al. 2017). Finally, recent studies have shown that birnessite-like phyllosulfates, which are the major Mn oxide phases in soils and sediments (Post 1999), transform into hollandite-like phases and other tunnel structures under ambient environmental conditions (Chen et al. 1986; Grangeon et al. 2014, 2015). The structural water inherited from the interlayers of these phyllosulfates end up in the tunnels as H₂O and as OH⁻, and the hydrous components of the hollandite-like phases are important factors in determining their capacities to exchange or accommodate various cations, such as Li⁺, Na⁺, Ba²⁺, Pb²⁺, and K⁺, in natural systems.

FUNDING

Funding for this work was provided by NSF EAR1925903. This research also utilized samples from the Smithsonian Mineral Research Collection at the Museum of Natural History. The FTIR laboratory at the Smithsonian Institution was established with generous support from Stephen Turner. This research used resources of the Advanced Photon Source, a U.S. Department of Energy (DOE) Office of Science User Facility operated for the DOE Office of Science by Argonne National Laboratory under Contract No. DE-AC02-06CH11357. ESI is supported by the PNNL managed Geosciences Research Program of the U.S. Department of Energy (DOE), Office of Basic Energy Sciences, Division of Chemical Sciences, Geosciences & Biosciences. The research was performed in part using the Environmental Molecular Sciences Laboratory (EMSL), a national scientific user facility sponsored by the U.S. DOE's Office of Biological and Environmental Research and located at Pacific Northwest National Laboratory (PNNL). PNNL is operated for DOE by Battelle Memorial Institute under Contract No. DE-AC06-76RLO-1830. We also acknowledge support from NSF EAR11-47728.

REFERENCES CITED

- Akkopru-Akgun, B., Trolier-McKinstry, S., and Lanagan, M.T. (2015) MnO₂ thin film electrodes for enhanced reliability of thin glass capacitors. *Journal of the American Ceramic Society*, 98, 3270–3279.
- Baur, W.H. (1972) Prediction of hydrogen bonds and hydrogen atom positions in crystalline solids. *Acta Crystallographica Section B Structural Crystallography and Crystal Chemistry*, 28, 1456–1465.
- Brown, G.E., Sueno, S., and Prewitt, C.T. (1973) A new single-crystal heater for the precession camera and four-circle diffractometer. *American Mineralogist*, 58, 698–704.
- Bruce, P.G., Freunberger, S.A., Hardwick, L.J., and Tarascon, J.-M. (2012) Li-O₂ and Li-S batteries with high energy storage. *Nature Materials*, 11, 19–29.
- Carmichael, S.K., Doctor, D.H., Wilson, C.G., Feierstein, J., and McAleer, R.J. (2017)

- New insight into the origin of manganese oxide ore deposits in the Appalachian Valley and Ridge of northeastern Tennessee and northern Virginia, U.S.A. *Geological Society of America Bulletin*, 129, B31682.1–1180.
- Chen, C.C., Golden, D.C., and Dixon, J.B. (1986) Transformation of synthetic bimesite to cryptomelane—an electron-microscopic study. *Clays and Clay Minerals*, 34, 565–571.
- Feng, Q., Kanoh, H., Miyai, Y., and Ooi, K. (1995) Alkali metal ions insertion/extraction reactions with hollandite-type manganese oxide in the aqueous phase. *Chemistry of Materials*, 7, 148–153.
- Grangeon, S., Lanson, B., and Lanson, M. (2014) Solid-state transformation of nano-crystalline phyllosilicates into tectomanganate: influence of initial layer and interlayer structure. *Acta Crystallographica Section B, Structural Science, Crystal Engineering and Materials*, 70, 828–838.
- Grangeon, S., Fernandez-Martinez, A., Warmont, F., Gloter, A., Marty, N., Poulain, A., and Lanson, B. (2015) Cryptomelane formation from nanocrystalline vernadite precursor: A high energy X-ray scattering and transmission electron microscopy perspective on reaction mechanisms. *Geochemical Transactions*, 16, 12.
- Gruner, J.W. (1943) The chemical relationship of cryptomelane (psilomelane), hollandite, and coronadite. *American Mineralogist*, 28, 497–506.
- Gutzmer, J., and Beukes, N.J. (2000) Asbestiform manjiroite and todorokite from the Kalahari manganese field, South Africa. *South African Journal of Geology*, 103, 163–174.
- Hammersley, A.P., Svensson, S.O., Hanfland, M., Fitch, A.N., and Hausermann, D. (1996) Two-dimensional detector software: From real detector to idealized image or two-theta scan. *High Pressure Research*, 14, 235–248.
- Ilton, E.S., Post, J.E., Heaney, P.J., Ling, F.T., and Kerisit, S.N. (2016) XPS determination of Mn oxidation states in Mn (hydr) oxides. *Applied Surface Science*, 366, 475–485.
- Johnson, C.S., Dees, D.W., Mansueti, M.F., Thackeray, M.M., Vissers, D.R., Argyriou, D., Loong, C.K., and Christensen, L. (1997) Structural and electrochemical studies of alpha-manganese dioxide ($\alpha\text{-MnO}_2$). *Journal of Power Sources*, 68, 570–577.
- Kijima, N., Takahashi, Y., Akimoto, J., and Awaka, J. (2005) Lithium ion insertion and extraction reactions with hollandite-type manganese dioxide free from any stabilizing cations in its tunnel cavity. *Journal of Solid State Chemistry*, 178, 2741–2750.
- Meisser, N., Perseil, E., Brugger, J., and Chiappero, P. (1999) Strontiomelane, $\text{SrMn}_4^{2+}\text{Mn}_2^{3+}\text{O}_{16}$, a new mineral species of the cryptomelane group from St. Marcel–Praborna, Aosta Valley, Italy. *Canadian Mineralogist*, 37, 673–678.
- Nambu, M., and Tanida, K. (1967) Manjiroite, new manganese dioxide mineral, from Kohare Mine, Iwate Prefecture, Japan. *The Journal of the Japanese Association of Mineralogists, Petrologists and Economic Geologists*, 58, 39–54.
- (1980) Cryptomelane–Manjiroite–Hollandite Series Minerals. *Journal of the Mineralogical Society of Japan*, 14, 62–85 (in Japanese).
- Post, J.E., and Bish, D.L. (1989) Rietveld refinement of the coronadite structure. *American Mineralogist*, 74, 913–917.
- Post, J.E., and Burnham, C.W. (1986) Modeling tunnel-cation displacements in hollandites using structure-energy calculations. *American Mineralogist*, 71, 1178–1185.
- Post, J.E. (1999) Manganese oxide minerals: crystal structures and economic and environmental significance. *Proceedings of the National Academy of Sciences of the United States of America*, 96, 3447–3454.
- Post, J.E., and Buchwald, V.F. (1991) Crystal structure refinement of akaganeite. *American Mineralogist*, 76, 272–277.
- Post, J.E., Von Dreele, R.B., and Buseck, P.R. (1982) Symmetry and cation displacements in hollandites: structure refinements of hollandite, cryptomelane and priderite. *Acta Crystallographica*, 38, 1056–1065.
- Post, J.E., Heaney, P.J., Von Dreele, R.B., and Hanson, J.C. (2003) Neutron and temperature-resolved synchrotron X-ray powder diffraction study of akaganeite. *American Mineralogist*, 88, 782–788.
- Potter, R.M., and Rossman, G.R. (1979) The tetravalent manganese oxides: identification, hydration, and structural relationships by infrared spectroscopy. *American Mineralogist*, 64, 1199–1218.
- Rietveld, H.M. (1969) A profile refinement method for nuclear and magnetic structures. *Journal of Applied Crystallography*, 2, 65–71.
- Rossouw, M.H., Liles, D.C., Thackeray, M.M., David, W.I.F., and Hull, S. (1992) Alpha manganese-dioxide for lithium batteries—A structural and electrochemical study. *Materials Research Bulletin*, 27, 221–230.
- Sauvage, F., Laffont, L., Tarascon, J.-M., and Baudrin, E. (2007) Study of the insertion/deinsertion mechanism of sodium into $\text{Na}_{0.44}\text{MnO}_2$. *Inorganic Chemistry*, 46, 3289–3294.
- Shannon, R.D. (1976) Revised effective ionic radii and systematic studies of interatomic distances in halides and chalcogenides. *Acta Crystallographica Section A*, 32, 751–767.
- Stephens, P.W. (1999) Phenomenological model of anisotropic peak broadening in powder diffraction. *Journal of Applied Crystallography*, 32, 281–289.
- Szymański, J.T. (1986) The crystal structure of mannardite, a new hydrated cryptomelane-group (hollandite) mineral with a doubled short axis. *Canadian Mineralogist*, 24, 67–78.
- Thompson, P., Cox, D.E., and Hastings, J.B. (1987) Rietveld refinement of Debye-Scherrer synchrotron X-ray data from Al_2O_3 . *Journal of Applied Crystallography*, 20, 79–83.
- Toby, B.H., and Von Dreele, R.B. (2013) GSAS-II: The genesis of a modern open-source all purpose crystallography software package. *Journal of Applied Crystallography*, 46, 544–549.
- Tompsett, D.A., and Islam, M.S. (2013) Electrochemistry of Hollandite $\alpha\text{-MnO}_2$: Li-Ion and Na-Ion Insertion and Li_2O Incorporation. *Chemistry of Materials*, 25, 2515–2526.
- Yang, Z., Trahey, L., Ren, Y., Chan, M.K.Y., Lin, C., Okasinski, J., and Thackeray, M.M. (2015) In situ high-energy synchrotron X-ray diffraction studies and first principles modeling of $\alpha\text{-MnO}_2$ electrodes in Li-O_2 and Li-ion coin cells. *Journal of Materials Chemistry A*, 3, 7389–7398.
- Yang, Z., Ford, D.C., Park, J.S., Ren, Y., Kim, S., Kim, H., Fister, T.T., Chan, M.K.Y., and Thackeray, M.M. (2017) Probing the Release and Uptake of Water in $\alpha\text{-MnO}_2 \cdot x\text{H}_2\text{O}$. *Chemistry of Materials*, 29, 1507–1517.
- Zhang, R., Yu, X., Nam, K.-W., Ling, C., Arthur, T.S., Song, W., Knapp, A.M., Ehrlich, S.N., Yang, X.-Q., and Matsui, M. (2012) $\alpha\text{-MnO}_2$ as a cathode material for rechargeable Mg batteries. *Electrochemistry Communications*, 23, 110–113.

MANUSCRIPT RECEIVED OCTOBER 11, 2020

MANUSCRIPT ACCEPTED APRIL 1, 2021

MANUSCRIPT HANDLED BY ADAM WALLACE

Endnote:

¹Deposit item AM-22-47848, Online Materials. Deposit items are free to all readers and found on the MSA website, via the specific issue's Table of Contents (go to http://www.minsocam.org/MSA/AmMin/TOC/2022/Apr2022_data/Apr2022_data.html). The CIF has been peer reviewed by our Technical Editors.